Anomalous parabolic equation results for propagation in leaky surface ducts

Michael B. Porter
Department of Mathematics and Center for Applied Mathematics and Statistics, New Jersey Institute of Technology, Newark, New Jersey 07102

Finn B. Jensen
SACLANT Undersea Research Centre, 19138 La Spezia, Italy

(Received 1 February 1993; accepted for publication 21 March 1993)

Surface ducts are formed by wind mixing at the sea surface and are a common feature in many of the world's oceans. These surface ducts have the effect of channeling acoustic energy for long ranges. This paper, however, focuses on the energy that leaks out of the surface duct—paths that are typically neglected by ray models. It is found that the leakage energy at lower frequencies can be surprisingly strong so that a receiver in a ray-theory shadow zone is actually well insonified. Furthermore, the leakage energy is refracted back into the duct where it may dominate the ducted paths. Inside the duct, these two arrivals add up constructively or destructively resulting in anomalously high or low acoustic levels in the surface duct relative to a prediction that neglects the leaky arrival. Thus, a full-wave model is needed; however, certain types of parabolic equations (PEs) fail for these problems because they scramble the phases of the two dominant arrivals. The same mechanism that causes the PEs to fail makes the problem very sensitive to environmental data. For instance, a change in the mean duct speed of 0.5 m/s can also produce large changes in the acoustic levels.

PACS numbers: 43.30.Bp, 43.30.Cq

INTRODUCTION

A common oceanographic feature is the so-called mixed layer that results from wind-driven mixing at the ocean surface. An introduction to the oceanographic and acoustic characteristics of surface ducts may be found in Ref. 1. A key feature of mixed layers is that they lead to a surface duct that traps acoustic energy. An example of such a problem is shown in Fig. 1. The sound-speed profile on the left shows a typical deep-water profile with the mixed layer leading to a small upward-refracting zone in the upper 250 m. The ray trace for a source in the surface duct (at a depth of 25 m) illustrates the two families of rays for such a source: First, there are rays that are trapped within the surface duct; second, there are rays with a steeper take-off angle that escape from the duct and form a convergence zone pattern with energy cycling up and down the channel and refocusing near the surface about every 50 km. A plot of the transmission loss at 80 Hz shown in Fig. 2 confirms the trapping effect of the surface duct. We also observe that there are bands of energy suggesting leakage out of the surface duct.

These features of surface-duct propagation are by now well known. Indeed, according to Urick[2] the acoustic effects of the surface duct were first studied by Steinberger in 1937. Since then, many other researchers have studied surface-duct propagation. In the early 1970s an extensive set of CW experiments was performed in the Surface-Duct Sonar Measurements (SUDS) program.[3] The issue of duct leakage is discussed in Refs. 4–8. Freese[9] discusses an interesting set of experimental results for impulsive sources in surface ducts. That work illustrates experimentally and numerically the importance of leakage in and out of the surface duct in a case similar to our own.

Our interest in this problem has been stimulated by an anomalous numerical result obtained in a routine modeling study. The profile that manifested the numerical problems is, in fact, that shown in Fig. 1.

The remainder of this paper is organized as follows. In Sec. I we present a set of numerical results using different models. The striking feature of these results is that they are derived from models in which most researchers would have had a high degree of confidence, yet there are large discrepancies in the results. In Sec. II we study this problem in the time domain using an impulsive signal. These results lead us to a clear physical interpretation of the propagation paths. With this insight we explain in Sec. III the difficult requirements imposed on any numerical model and consequently why certain parabolic equations (PEs) fail and others do not. In Sec. IV we end with a summary and conclusions.

I. NUMERICAL RESULTS

Figure 3 shows the numerical results that prompted this study. The solid line in all the plots is a reference solution obtained using the SNAP normal mode code.[10] This solution agrees to within a line width with solutions obtained using KRAKEN[11] and a spectral integral code. The receiver depth for these calculations was 100 m. The dashed line in Fig. 3(a) is the result obtained using the Thomson–Chapman PE.[12,13] The somewhat startling aspect of this result is that it shows a discrepancy reaching 15 dB. Furthermore, the error is not confined to a narrow

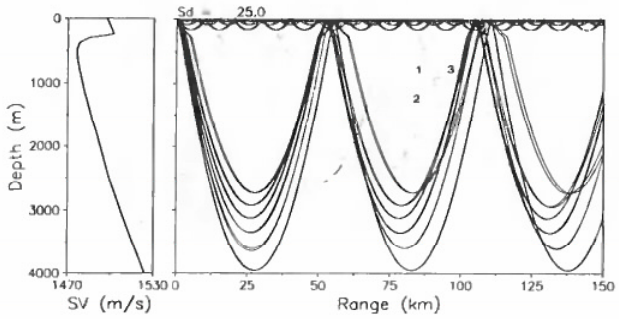

FIG. 1. Sound-speed profile and corresponding ray trace.

region but averages about 7 dB over the entire region between the first and second convergence zones. A concern that often arises with PEs is whether they are sufficiently wide-angle. However, in this case the propagating rays cover a narrow spectrum of about $\pm 15°$. Figure 3(b) shows the result obtained using the LOGPE,[14] which also shows a disturbingly large error.

This unexpected error became even more mysterious when we ran the standard Tappert–Hardin PE[15,16] yielding the excellent agreement shown in Fig. 3(c). This is the original narrow-angle version introduced into underwater acoustics in 1973. Today it has largely been replaced by models such as the Thomson–Chapman PE or LOGPE that have established a consistently better record in terms of accuracy. The Tappert–Hardin PE has been extended to wider angles by including additional terms in the Padé series approximation to the square-root operator. One such PE, the Claerbout PE, yields the result shown in Fig. 3(d), which also shows excellent agreement.

II. TIME-DOMAIN INTERPRETATION

To understand the peculiarities of the transmission loss results obtained using different PEs we performed some broadband calculations. A simple wavelet was used for the source function and then observed on vertical and horizontal "arrays" positioned at different locations in the waveguide.

The objective of looking at time-domain results was to observe differences in the arrival structure with the different PE models, thus obtaining clues to the possible failure mechanism. Interestingly there were no *visible* differences between the arrival structure as calculated by the four different PEs and the normal mode model. We will discuss this apparent inconsistency later.

Figure 4 shows the predicted arrival structure for a horizontal "array" with hydrophones spaced every 10 km and within the surface duct. The pulse amplitudes are multiplied by range to compensate for geometrical spreading and attenuation. The horizontal axis shows a reduced time in which the pulses have been shifted in time based on an average propagation speed of 1510 m/s. These calculations were done by running the normal mode code over a sweep of frequencies. The complex pressure fields were then added up with a weighting factor based on the source spectrum to obtain the time series of the received signal (Fourier synthesis).

The principal propagation paths are illustrated in Fig. 1. The first arrival corresponds to a ray trapped in the surface duct. The ray is refracted in a part of the ocean with a high average sound speed and therefore arrives first. At a range of about 50 km we see a second arrival coming in that corresponds to a convergence zone path. Interestingly this arrival is present well past the actual convergence zone. As indicated in Fig. 1, it is identified with a "leaky CZ" path, that is, a ray path that leaks out of the surface duct and then is refracted like an ordinary CZ path. This duct-leakage phenomenon is well-known. An important and seemingly unappreciated aspect of such paths is that they can lead to an extremely strong arrival as shown in the plot of Fig. 4. Note that the leaky CZ arrival is actually stronger than the surface-duct arrival. Furthermore, we tend to think of the energy leaking out of the

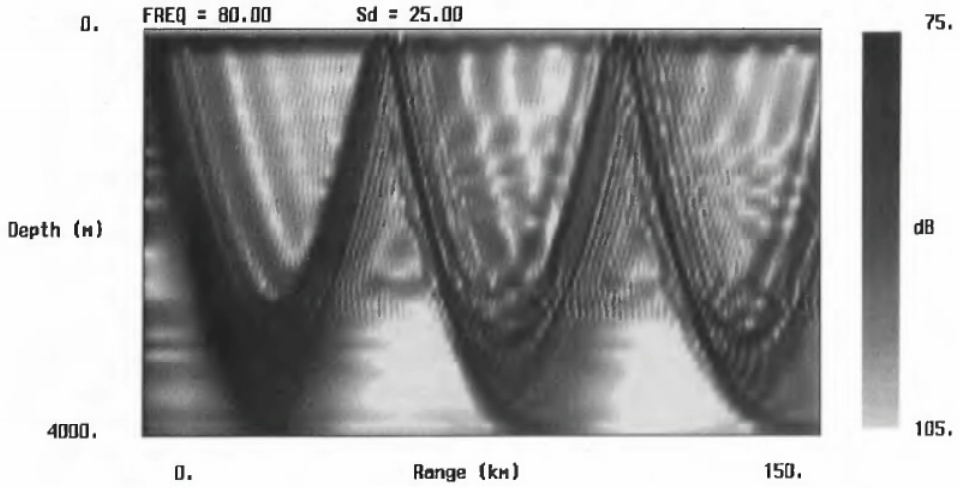

FIG. 2. Transmission loss for the mixed-layer profile.

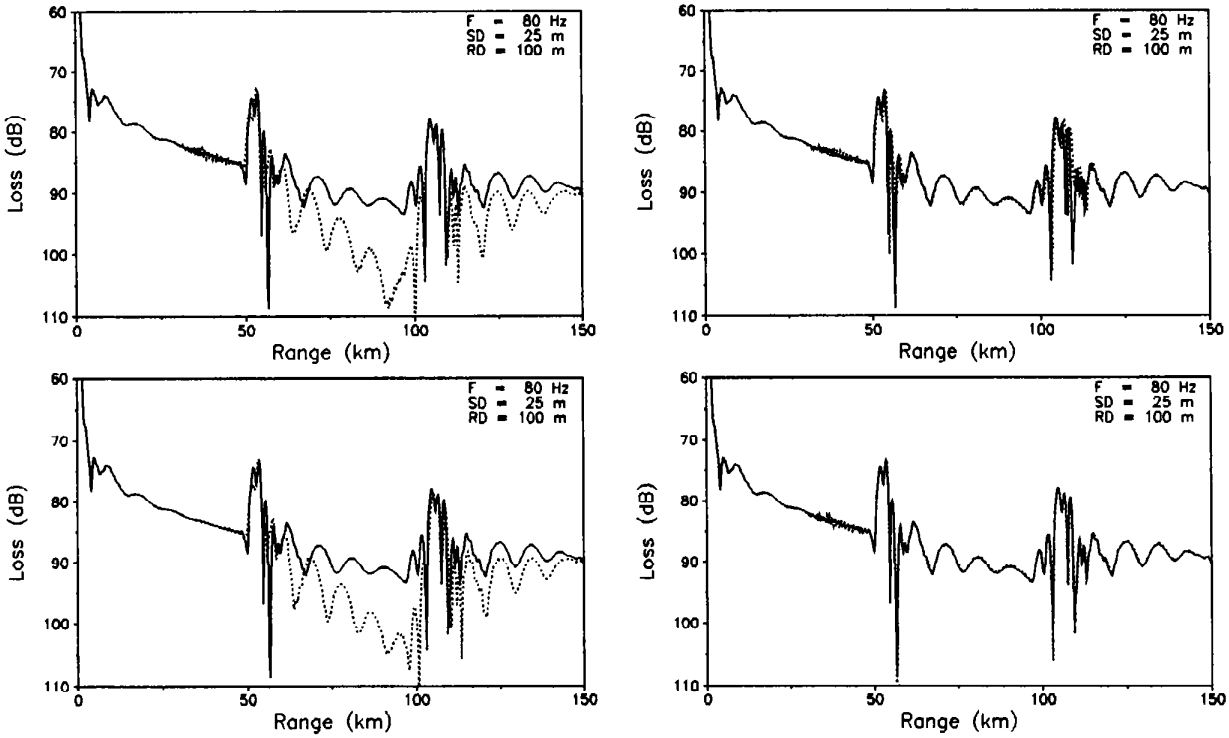

FIG. 3. Comparison of PE (---) to exact (———) solution. (a) Thomson–Chapman, (b) LOGPE, (c) Tappert–Hardin, (d) Claerbout.

surface duct as if it simply leaves the waveguide while in fact the leakage arrival is refracted by the water column and can refocus at other ranges.

Finally, we observe that there is a third arrival showing up at the second convergence zone (at about 100 km).

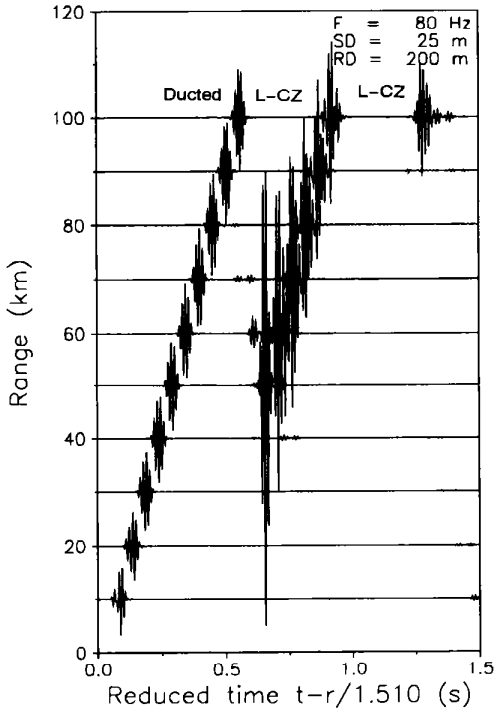

FIG. 4. Arrival structure versus range for a receiver in the duct.

This is, of course, the second cycle of the convergence zone path. Beyond this range the arrival structure becomes increasingly complicated, involving various combinations of leaky and ducted paths.

A slightly different view is obtained if we sample the field with a vertical "array" extending from the surface to a depth of 1000 m and placed at a range of 80 km. The resulting arrival structure is shown in Fig. 5. The trace for the receiver in the surface duct (100 m) shows the pattern we have already seen on the horizontal array. The first arrival is a ducted path and the second arrival is a leaky CZ path. As we go to deeper hydrophones we see the ducted arrival becomes a leaky arrival. The leaky CZ, on the other hand, splits into two arrivals—one coming to the receiver from below and the other from above. Taking a different view, we can say that the strong leaky CZ path observed in the surface duct is obtained when those same two paths coalesce.

With these and other glimpses of the field we obtain a complete picture of the important propagation paths. We can now observe that there is a stringent accuracy requirement for any propagation model: It must accurately predict the relative arrival times to within hundredths of a second to give an accurate prediction in the region between the first and second convergence zones (and beyond). Within this region we have seen that there are two arrivals of comparable strength. Thus, if we look at a single frequency the relative phase leads to constructive or destructive interference depending on the details of the profile.

At a center frequency of 80 Hz, it takes only a difference of about 6 ms in the travel time to shift the phase by

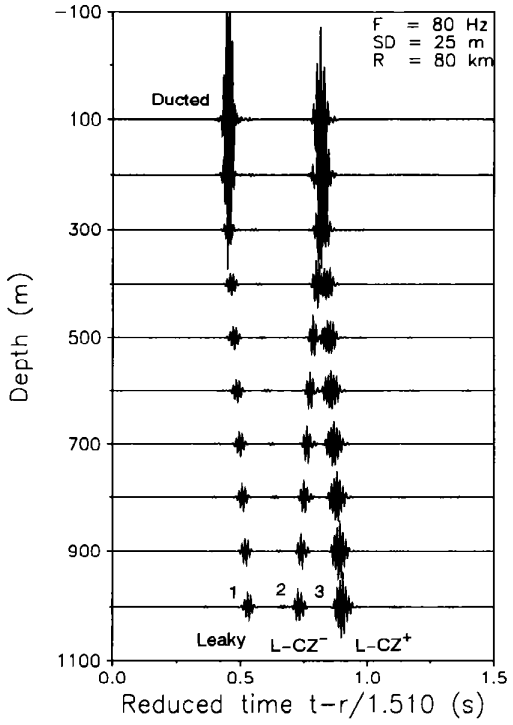

FIG. 5. Arrival structure versus depth in the second convergence zone.

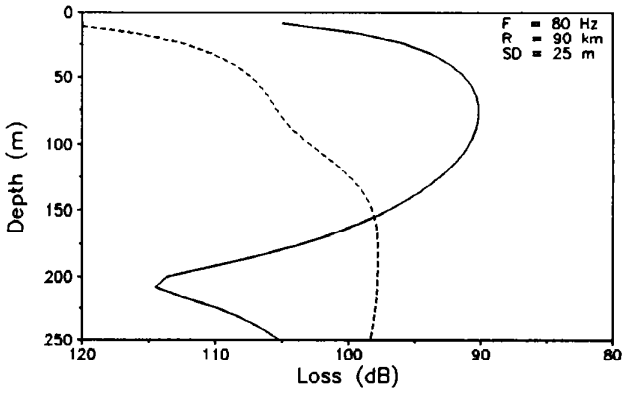

FIG. 6. Transmission loss versus range in the second convergence zone. (———), original problem; (---), perturbed problem.

180°. Such differences in arrival time are not visible on the scales used for plotting the time series, which explains why there were no visible differences between the times series plots of the PEs.

Of course, ocean acoustic problems are characterized by multipath propagation. What is then unique about this particular multipath case? The answer is that the two paths involved maintain a nearly constant difference in travel time throughout the region from the first to the second convergence zone. (This may be seen geometrically from Fig. 1.) As a result, the transmission loss shows a smooth behavior. Furthermore, any phase error affects that whole region almost uniformly. It is this mechanism that gives the impression that energy levels are low in the surface duct in some of the PE results. It is also this mechanism that makes the PE error so unexpected. That is, PEs are well-known to generate phase errors. These errors are usually seen as erratic deviations in the pattern of the transmission loss. The consistent *level* error is what is unexpected.

An interesting consequence of this explanation is that the physical problem is itself very sensitive to small changes. Thus, if we take our reliable normal mode model and make a small change in the mixed-layer speed we can induce a large change in the transmission loss. For instance, in Fig. 6 we have increased the speed by just 0.5 m/s. The effect of this is to reduce the travel time for the ducted arrival relative to that of the leaky CZ arrival. The solid and dotted curves show the enormous change in transmission loss that results. We should emphasize that what we are looking at here is not a model error but the extreme sensitivity of the results to small changes in the environment.

III. PE TYPES

The preceding section provided a fairly clear picture of the accuracy requirements for any acoustic model: It must be able to accurately predict the relative travel time of the two important paths. The remaining mystery is why do some of the PEs work and others not? After all, the PEs all have phase errors so why should any of them work? In brief, the answer is that the PEs can make serious phase errors provided the same phase error is made for both of the critical paths. In other words, it is the *relative* travel time that is important, not the absolute travel time.

In Sec. I, we saw that the Tappert–Hardin PE and the Claerbout PE both gave an accurate prediction. These PEs are members of the wider class of Padé PEs. Let us recall the derivation following the operator notation of Ref. 17. The starting point is the Helmholtz equation for a constant-density medium in cylindrical coordinates (r,z,ϑ) and for a harmonic point source of time dependence $\exp(-i\omega t)$:

$$\frac{\partial^2 p}{\partial r^2}+\frac{1}{r}\frac{\partial p}{\partial r}+\frac{\partial^2 p}{\partial z^2}+k_0^2 n^2 p=0, \tag{1}$$

where we have assumed azimuthal symmetry and hence no dependence on the ϑ coordinate. Here, $p(r,z)$ is the acoustic pressure, $k_0=\omega/c_0$ is a reference wave number, and $n(r,z)=c_0/c(r,z)$ is the index of refraction. We next introduce a new dependent variable $u(r,z)$ with the cylindrical spreading removed,

$$p(r,z)=u(r,z)/\sqrt{r}, \tag{2}$$

and make the far-field approximation to obtain

$$(P^2+k_0^2 Q^2)u=0, \tag{3}$$

where

$$P=\frac{\partial}{\partial r}, \quad Q=\sqrt{\frac{1}{k_0^2}\frac{\partial^2}{\partial z^2}+n^2}. \tag{4}$$

The next step is to factor this equation into two components, an outgoing and an incoming wave component, according to

$$(P-ik_0Q)(P+ik_0Q)u-ik_0[P,Q]u=0, \tag{5}$$

where

$$[P,Q]u=PQu-QPu \tag{6}$$

is the so-called commutator of the operators P and Q. For range-independent media where $n\equiv n(z)$, the two operators commute and the last term in Eq. (5) is equal to zero. Selecting only the outgoing wave component, we then obtain

$$Pu=ik_0Qu$$

or

$$\frac{\partial u}{\partial r}=ik_0\left(\sqrt{\frac{1}{k_0^2}\frac{\partial^2}{\partial z^2}+n^2}\right)u. \tag{7}$$

This equation is a genuine one-way wave equation, that for range-independent environments invokes only the far-field approximation. However, to use it we must interpret the square-root operator that occurs. For convenience we write Q given by Eq. (4) as

$$Q=\sqrt{1+q}, \tag{8}$$

where

$$q=\frac{1}{k_0^2}\frac{\partial^2}{\partial z^2}+n^2-1. \tag{9}$$

A solvable parabolic wave equation is now obtained by making a Taylor series expansion of Q:

$$\sqrt{1+q}=1+\frac{q}{2}-\frac{q^2}{8}+\frac{q^3}{16}+\cdots. \tag{10}$$

If we retain only the first two terms we get the following approximate form of the square-root operator:

$$Q\simeq 1+\frac{q}{2}=1+\frac{1}{2k_0^2}\frac{\partial^2}{\partial z^2}+\frac{n^2-1}{2}. \tag{11}$$

Substituting this expression for Q into the generalized one-way wave equation [Eq. (7)], we obtain

$$\frac{\partial u}{\partial r}=\frac{ik_0}{2}\left(\frac{1}{k_0^2}\frac{\partial^2}{\partial z^2}+n^2+1\right)u, \tag{12}$$

which is the standard PE. [Although, for numerical reasons the standard PE is often written in terms of a new variable $\psi=u\exp(-ik_0r)$.]

The above derivation based on a series expansion of the square-root operator Q suggests many ways to formulate better PE approximations with a wide-angle capability. The wide-angle Claerbout[18] equation uses

$$\sqrt{1+q}\simeq\frac{1+0.75q}{1+0.25q}. \tag{13}$$

Still higher-order expansions are obtained using more terms in the Padé series expansion:

$$\sqrt{1+q}=1+\sum_{j=1}^{l}\frac{a_{j,l}q}{1+b_{j,l}q}+O(q^{2l+1}), \tag{14}$$

where l is the number of terms in the expansion. The coefficients are computed to yield a good approximation to the square root. One such choice is

$$a_{j,l}=\frac{2}{2l+1}\sin^2\left(\frac{j\pi}{2l+1}\right),\quad b_{j,l}=\cos^2\left(\frac{j\pi}{2l+1}\right).$$

This general Padé series approach was proposed by Bamberger *et al.*[19] and first implemented by Collins.[20] It is instructive to write out this expansion when including one term only from the sum:

$$\sqrt{1+q}\simeq 1+\frac{0.50q}{1+0.25q}, \tag{15}$$

which is easily seen to be equivalent to the expansion given in Eq. (13). Thus, the Padé series includes as a special case the Claerbout PE form.

Substituting the general Padé series approximation to the square root of Eq. (14) into the one-way equation of Eq. (7) we obtain the generalized very-wide-angle PE

$$\frac{\partial u}{\partial r}=ik_0\left(1+\sum_{j=1}^{l}\left\{\left[a_{j,l}\left(\frac{1}{k_0^2}\frac{\partial^2}{\partial z^2}+n^2-1\right)\right]\times\left[1+b_{j,l}\left(\frac{1}{k_0^2}\frac{\partial^2}{\partial z^2}+n^2-1\right)\right]^{-1}\right\}\right)u, \tag{16}$$

which can be solved by finite-difference or finite-element techniques.

A key point about the Padé PE family is that the PE modes are closely tied to the Helmholtz modes. Let $Z_m(z)$ and k_m denote the eigenfunctions and eigenvalues for the equation

$$\frac{d^2}{dz^2}Z_m(z)+(k_0^2n^2-k_m^2)Z_m(z)=0. \tag{17}$$

We assume the boundary conditions are such that the eigenfunctions form a complete set. Then, if we seek a solution of the Padé PE in the form

$$u(r,z)=\sum_{m=1}^{\infty}Z_m(z)R_m(r), \tag{18}$$

and make use of the orthogonality of the eigenfunctions, we find

$$R_m'(r)=ik_0\left(1+\sum_{j=1}^{l}\frac{a_{j,l}(k_m^2/k_0^2-1)}{1+b_{j,l}(k_m^2/k_0^2-1)}\right)R_m(r). \tag{19}$$

Therefore,

$$R_m(r)\propto\exp\left[ik_0\left(1+\sum_{j=1}^{l}\frac{a_{j,l}(k_m^2/k_0^2-1)}{1+b_{j,l}(k_m^2/k_0^2-1)}\right)r\right]. \tag{20}$$

Note that if we pass to the limit $l\to\infty$ the Padé series converges to $\sqrt{1+(k_m^2/k_0^2-1)}=k_m/k_0$ and we obtain

$$R_m(r)\propto\exp(ik_mr). \tag{21}$$

Similarly, we can use these same eigenfunctions to find a solution of the original Helmholtz equation. We substitute in Eq. (1) and obtain the well-known normal mode representation of the solution

$$p(r,z) = \sum_{m=1}^{\infty} Z_m(z) R_m^{\mathrm{HE}}(r), \tag{22}$$

where

$$R_m^{\mathrm{HE}}(r) \propto H_0^{(1)}(k_m r). \tag{23}$$

Taking the far-field approximation to the Hankel function and removing the cylindrical spreading term, we obtain

$$u^{\mathrm{HE}}(r,z) = \sum_{m=1}^{\infty} Z_m(z) R_m^{\mathrm{HE}}(r), \tag{24}$$

where

$$R_m^{\mathrm{HE}}(r) \propto \exp(ik_m r). \tag{25}$$

Thus, the Helmholtz equation and the Padé PE have identical depth eigenfunctions $Z_m(z)$. However, comparing the Padé range term given in Eq. (20) to the Helmholtz result given in Eq. (25) we see that there is a phase error that goes to zero as the number of terms in the Padé series goes to infinity. This extends a result obtained by McDaniel[21] for the standard PE.

The significance of this is the following. The two paths that contribute in the surface duct are associated with points in the k spectrum that are very near to each other. That is, the rays for the two paths have nearly identical take-off angles and may be associated with a single mode in the modal sum. Furthermore, Eq. (20) shows that the phase error of the Padé PE is a constant function of depth for an individual mode. Thus, the phase errors are nearly identical for the two paths and the Padé family of PEs does an excellent job of predicting the interference within the surface duct.

The remaining question is why do the Thomson–Chapman PE and the LOGPE do poorly on this problem. We have just seen that the Padé family of PEs have a special angle-sensitive error that allows them to work. Conversely, it is not hard to demonstrate that both the Thomson–Chapman PE and the LOGPE induce phase errors along a ray path that depend not simply on the take-off angle of the ray, but on the particular characteristics of the medium that the ray passes through. Since the phase errors of the two paths are not locked, then the individual phases must be propagated with extremely high accuracy.

Parabolic equation models that are not members of the Padé family may still give the correct result for such problems if they are tuned to provide the relative phase of the arrivals correctly. Indeed if the reference sound speed c_0 is chosen appropriately, the Thomson–Chapman PE will give the correct result. For the moment, the only way to choose this parameter is via an intermodel comparison, which clearly is not helpful.

IV. SUMMARY

We find several interesting features of surface-duct propagation with important implications for numerical modeling. First, the leakage energy that is often ignored can be surprisingly strong at lower frequencies. Second, it stays in the waveguide refracting up and down the ocean channel and forming a leaky CZ arrival. After the first convergence zone we find that the field is composed of two arrivals: a classical ducted arrival and the leaky CZ arrival. An accurate model prediction requires an accurate prediction of the relative phase of these two arrivals. This poses a severe accuracy requirement on the computer model as well as a severe accuracy requirement in terms of environmental knowledge.

The importance of this interference effect depends critically on the way the data are processed. Thus, as discussed earlier, the small errors in the relative travel times were not visible in the time series plots produced by the PEs. Similarly, for band-averaged transmission loss the relative phases are less important so there is less sensitivity to the environmental knowledge.

Another interesting implication of this study is that traditional ray models that neglect the leaky arrival altogether will perform poorly under these conditions. These results have important implications for sonar system modeling. A source in the ray-theory shadow zone may actually insonify the surface duct quite effectively. Similarly, a receiver in the shadow zone may sense a strong field from a source in the surface duct.

ACKNOWLEDGMENTS

This work was supported in part by the Office of Naval Research under Contract No. N00014-92-J and by the Naval Research Laboratory under Contract No. N00014-91-J-2020.

[1] M. B. Porter, S. Piacsek, L. Henderson, and F. B. Jensen, "Surface duct propagation and the ocean mixed layer," in *Coupled Ocean Prediction and Acoustic Propagation Models*, edited by A. Robinson and D. Lee (AIP, New York, 1993).

[2] R. J. Urick, *Principles of Underwater Sound* (McGraw-Hill, New York, 1983), 3rd ed.

[3] E. R. Anderson and M. A. Pedersen, "Surface-duct sonar measurements," Rep. NUC TP-463, Naval Undersea Center, San Diego, CA (1976).

[4] D. E. Weston, C. G. Esmond, and A. Ferris, "The duct leakage relation for the surface sound channel," J. Acoust. Soc. Am. **89**, 156–164 (1991).

[5] P. A. Nysen and P. Scully-Power, "Sound propagation through an East Australian Current eddy," J. Acoust. Soc. Am. **63**, 1381–1388 (1978).

[6] F. M. Labianca, "Normal modes, virtual modes, and alternative representations in the theory of surface-duct sound propagation," J. Acoust. Soc. Am. **53**, 1137–1147 (1973).

[7] E. L. Murphy and J. A. Davis, "Modified ray theory for bounded media," J. Acoust. Soc. Am. **56**, 1747–1760 (1974).

[8] E. L. Murphy, "Modified ray theory for the two-turning-point problem," J. Acoust. Soc. Am. **47**, 899–908 (1970).

[9] H. A. Freese, "A comparison of multipath arrival structures observed in the presence of a surface duct with predictions obtained using classical ray techniques and the parabolic equation method," Rep. TM-811061, Naval Underwater System Center, New London, CT (1985).

[10] F. B. Jensen and M. C. Ferla, "SNAP: The SACLANTCEN normal-mode acoustic propagation model," Rep. SM-121, SACLANT Undersea Research Centre, La Spezia, Italy (1979).

[11] M. B. Porter and E. L. Reiss, "A numerical method for ocean acoustic normal modes," J. Acoust. Soc. Am. **76**, 244–252 (1984).
[12] D. J. Thomson and N. R. Chapman, "A wide-angle split-step algorithm for the parabolic equation," J. Acoust. Soc. Am. **74**, 1848–1854 (1983).
[13] M. D. Feit and J. A. Fleck, Jr., "Light propagation in graded-index fibers," Appl. Opt. **17**, 3990–3998 (1978).
[14] D. H. Berman, E. B. Wright, and R. N. Baer, "An optimal PE-type wave equation," J. Acoust. Soc. Am. **86**, 228–233 (1989).
[15] R. H. Hardin and F. D. Tappert, "Applications of the split-step Fourier method to the numerical solution of nonlinear and variable coefficient wave equations," SIAM Rev. **15**, 423 (1973).
[16] F. D. Tappert, "The parabolic approximation method," in *Wave Propagation in Underwater Acoustics*, edited by J. B. Keller and J. S. Papadakis (Springer-Verlag, New York, 1977), pp. 224–287.
[17] J. A. Davis, D. White, and R. C. Cavanagh, "NORDA parabolic equation workshop," Rep. TN-143, Naval Ocean Research and Development Activity, Stennis Space Center, MS (1982).
[18] J. F. Claerbout, *Fundamentals of Geophysical Data Processing* (Blackwell, Oxford, UK, 1985), pp. 194–207.
[19] A. Bamberger, B. Engquist, L. Halpern, and P. Joly, "Higher order parabolic wave equation approximations in heterogeneous media," SIAM J. Appl. Math. **48**, 129–154 (1988).
[20] M. D. Collins, "Applications and time-domain solution of higher-order parabolic equations in underwater acoustics," J. Acoust. Soc. Am. **86**, 1097–1102 (1989).
[21] S. T. McDaniel, "Propagation of normal mode in the parabolic approximation," J. Acoust. Soc. Am. **57**, 307–311 (1975).